B directly cleaves caspases and activates the apoptotic-signaling pathway in target cells [32, 33]. To evaluate the cytotoxic capability of each NK-cell subset, we examined the secretion of granzyme B in response to IL-12 or IL-18. Production of granzyme B by Ly6C^{high} NK cells was lower than that by Ly6C^{low} NK cells when stimulated with IL-12 or IL-18 (Fig. 3B). In addition, we examined CD107a expression in each NK-cell subset when cocultured with YAC-1 cells. CD107a is a glycoprotein present in the membrane of cytotoxic granules and exposed on the surface of activated NK cells [34]. Consistent with granzyme B productions, the percentage of CD107a$^+$ cells in Ly6C^{high} NK cells was lower than that in Ly6C^{low} NK cells when stimulated with IL-18 (Fig. 3C). These data collectively indicate that Ly6C^{low} NK cells exhibit stronger NK functions than do Ly6C^{high} NK cells in response to cytokine stimulation. These results correlated with our finding that Ly6C^{high} NK cells express higher levels of KLRG1, Ly49C/I, and lower levels of Ly108 (Fig. 2B). Therefore, Ly6C^{high} NK cells are thought to be refractory to cytokine stimulation.

Ly6C^{low} NK cells become Ly6C^{high} NK cells in the steady state

We next investigated the interrelationship of Ly6C^{low} and Ly6C^{high} NK cells. To determine whether these NK-cell subsets are interconvertible, we performed an in vivo transplantation assay. NK-cell subsets were sorted from the spleens of CD45.2 C57BL/6J (C57BL/6) mice and adoptively transferred into nonirradiated CD45.1 congenic mice by i.v. injection. Two weeks after the transplantation, we isolated the transferred CD45.2$^+$ NK cells from the spleen and examined their expression levels of Ly6C. Approximately 30% of CD45.2$^+$ NK cells in mice that received Ly6C^{low} NK cells were Ly6C^{high}, indicating that a significant portion of the transferred Ly6C^{low} NK cells were converted to Ly6C^{high} NK cells (Fig. 4A and B). In contrast, almost all transferred Ly6C^{high} NK cells did not change their high expression levels of Ly6C (Fig. 4A and B). These results suggest that Ly6C^{low} NK cells become Ly6C^{high} NK cells, but not vice versa in the steady state.

IL-15 converts Ly6C^{high} NK cells to Ly6C^{low} NK cells

IL-15 is a major cytokine required for the development and proliferation of NK cells [31, 35, 36]. To determine whether IL-15 affects the Ly6C expression levels of NK cells, both Ly6C^{low} and Ly6C^{high} NK cells were sorted and cultured with IL-15. First, we determined the absolute cell number of Ly6C^{low} and Ly6C^{high} NK cells. After 6-day culture, both subsets survived and Ly6C^{low} NK cells showed significantly higher proliferative potential than Ly6C^{high} NK cells (Fig. 5A). Next, we examined the expression levels of Ly6C at indicated time points. The Ly6C expression levels in Ly6C^{low} NK cells remained unchanged (Fig. 5B, left panel). Interestingly, however, the Ly6C expression levels of Ly6C^{high} NK cells gradually decreased, and about a half of the NK cells expressed Ly6C at

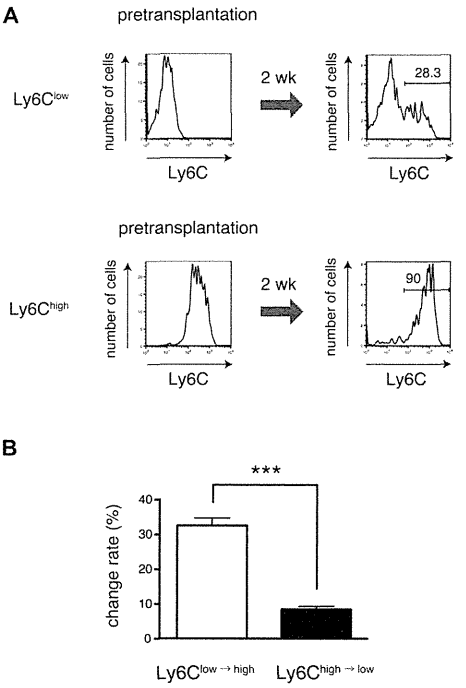

Figure 4. Ly6C^{high} NK cells are derived from Ly6C^{low} NK cells. (A and B) CD49b$^+$CD11b$^+$CD3e$^-$Ly6C^{low} NK cells and CD49b$^+$CD11b$^+$CD3e$^-$Ly6C^{high} NK cells were sorted from the spleen of CD45.2 C57BL/6 mice and transferred into nonirradiated CD45.1 congenic mice. Two weeks later, cells were harvested from the spleens of the recipient mice, stained for CD49b, CD11b, CD3e, CD45.2, and Ly6C and analyzed by flow cytometry. (A) The histogram plots show Ly6C expression profiles gated on CD49b$^+$CD11b$^+$CD3e$^-$CD45.2$^+$ cells. Numbers indicate percentage of Ly6C-positive cells. Data shown are from a single experiment representative of three independent experiments performed. (B) The graph indicates change rate of each subset (i.e., the percentage of Ly6C^{high} NK cells derived from Ly6C^{low} NK cells or Ly6C^{low} NK cells derived from Ly6C^{high} NK cells). Data shown are the means + SEM of three independent experiments performed. These data were compared using Student's two-tailed *t*-test. $^{***}p < 0.001$.

middle levels (Ly6C$^{mid(high)}$ NK cells) when cultured with IL-15 for 4 days, and finally many NK cells became Ly6C^{low} NK cells after 6 days in culture with IL-15 (Fig. 5B, right panel). Furthermore, we examined the effect of IL-2 on the expression levels of Ly6C, as IL-2 and IL-15 share the common cytokine-receptor gamma chain and IL-2 is also a major cytokine required for the development and proliferation of NK cells. After 6-day culture with IL-2, both subsets survived and Ly6C^{low} NK cells showed significantly higher proliferative capacity than Ly6C^{high} NK cells (Supporting Information Fig. 2A). Ly6C expression levels of Ly6C^{high} NK cells decreased and approximately half of the NK cells expressed Ly6C at intermediate levels (Supporting Information Fig. 2B). These results suggest that IL-2 also has the effect to convert Ly6C^{high} NK cells to Ly6C^{low} NK cells. However, the effect of IL-2 was not so strong as that of IL-15. Because the functions of the Ly6C^{low} NK cells were higher than those of the Ly6C^{high} NK cells (Fig. 3), we analyzed the effector functions of Ly6C^{low} NK cells derived from Ly6C^{low} NK cells (Ly6C$^{low(low)}$ NK cells) and of Ly6C$^{mid(high)}$ NK cells or Ly6C^{low}

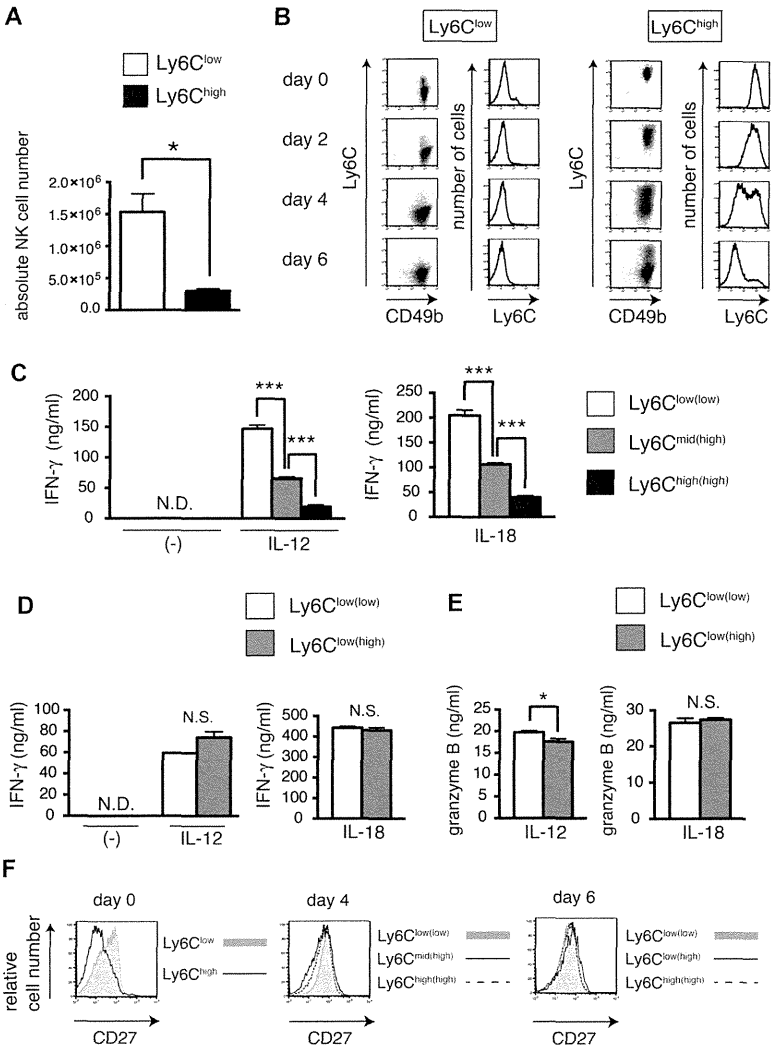

Figure 5. Conversion of Ly6C^{high} NK cells to Ly6C^{low} NK cells. (A) CD49b$^+$CD11b$^+$CD3e$^-$Ly6C^{low} NK cells and CD49b$^+$CD11b$^+$CD3e$^-$Ly6C^{high} NK cells (3×10^5) were cultured with IL-15 (100 ng/mL) for 6 days and absolute cell number was determined in triplicate cultures by using a 0.4% Trypan blue solution. Data are shown as means + SEM of three samples from a single experiment representative of three independent experiments. (B) CD49b$^+$CD11b$^+$CD3e$^-$Ly6C^{low} NK cells and CD49b$^+$CD11b$^+$CD3e$^-$Ly6C^{high} NK cells were cultured with IL-15 (100 ng/mL) for the indicated time periods. During each time period, cells were harvested and stained for CD49b, CD11b, CD3e, and Ly6C. Data shown are from a single experiment representative of three independent experiments performed. (C) NK-cell subsets were cultured with IL-15 (100 ng/mL) for 4 days. Ly6C$^{low(low)}$ NK cells, Ly6C$^{mid(high)}$ NK cells, and Ly6C$^{high(high)}$ NK cells were sorted by cell sorter and stimulated with IL-12 (100 ng/mL) or IL-18 (100 ng/mL) in the presence of IL-2 (100 ng/mL) (2×10^4 cells/well). After 24 h of incubation, the levels of IFN-γ in the culture supernatants were measured by ELISA. Data are shown as means + SEM of three samples from a single experiment representative of three independent experiments. (D, E) NK-cell subsets were cultured with IL-15 (100 ng/mL) for 7 days. Ly6C$^{low(low)}$ NK cells and Ly6C$^{low(high)}$ NK cells were then sorted and stimulated with IL-12 (100 ng/mL) or IL-18 (100 ng/mL) in the presence of IL-2 (100 ng/mL) (2×10^4 cells/well). After 24 h of incubation, the levels of (D) IFN-γ and (E) granzyme B in the culture supernatants were measured by ELISA. Data are shown as means + SEM of three samples from a single experiment representative of three independent experiments. (F) NK-cell subsets were cultured with IL-15 (100 ng/mL) for 4 or 6 days. The histogram plots show CD27 expression profiles gated on CD49b$^+$CD3e$^-$Ly6C$^{low/mid/high}$ cells. Data shown are a representative of two independent experiments. $^*p < 0.005$, $^{***}p < 0.001$. N.D., not detected, N.S., not significant (Student's two-tailed t-test).

NK cells derived from Ly6C^{high} NK cells (Ly6C$^{low(high)}$ NK cells) 4 days or 1 week in culture with IL-15, respectively. We found that the ability of Ly6C$^{mid(high)}$ NK cells to secrete IFN-γ was lower than that of Ly6C$^{low(low)}$ NK cells in response to IL-12 or IL-18 (Fig. 5C). Notably, approximately half of the Ly6C^{high} NK cells retained high expression levels of Ly6C (Ly6C$^{high(high)}$ NK cells) 4 days in culture with IL-15, and the production of IFN-γ of Ly6C$^{mid(high)}$ NK cells was higher than Ly6C$^{high(high)}$ NK cells (Fig. 5C). The ability of Ly6C$^{low(high)}$ NK cells to secrete IFN-γ and granzyme B was increased to levels comparable to that of Ly6C$^{low(low)}$ NK cells for 1 week in the presence of IL-15 (Fig. 5D and E). As stated above, Ly6C^{high} NK cells displayed lower proportions of cells expressing CD27 than did Ly6C^{low} NK cells before culture with IL-15 (Fig. 2D). We therefore examined CD27 expression levels of both Ly6C^{low} and Ly6C^{high} NK cells in culture with IL-15 for 4 days, and found no differences in the expression levels of CD27 among the three populations of Ly6C$^{low(low)}$, Ly6C$^{mid(high)}$, and Ly6C$^{high(high)}$ NK cells (Fig. 5F). Furthermore, after 6 days in culture, there was also no difference in the expression levels of CD27 among the three populations, Ly6C$^{low(low)}$, Ly6C$^{low(high)}$, and Ly6C$^{high(high)}$ NK cells. These results indicate that the expression levels of CD27 are not well correlated with activity of mature NK cells.

Conversion of Ly6C^{high} NK cells to Ly6C^{low} NK cells in vivo

We next examined whether Ly6C^{high} NK cells could become Ly6C^{low} NK cells in vivo. Because IL-15 was shown to convert Ly6C^{high} NK cells into Ly6C^{low} NK cells in vitro (Fig. 5B), we first performed an in vivo transplantation assay by overexpressing IL-15 in mice. To express IL-15 in vivo, we utilized the hydrodynamic tail vein injection method [37–39]. NK-cell subsets were sorted from the spleens of CD45.2 C57BL/6 mice and adoptively transferred into CD45.1 congenic mice injected with control vector

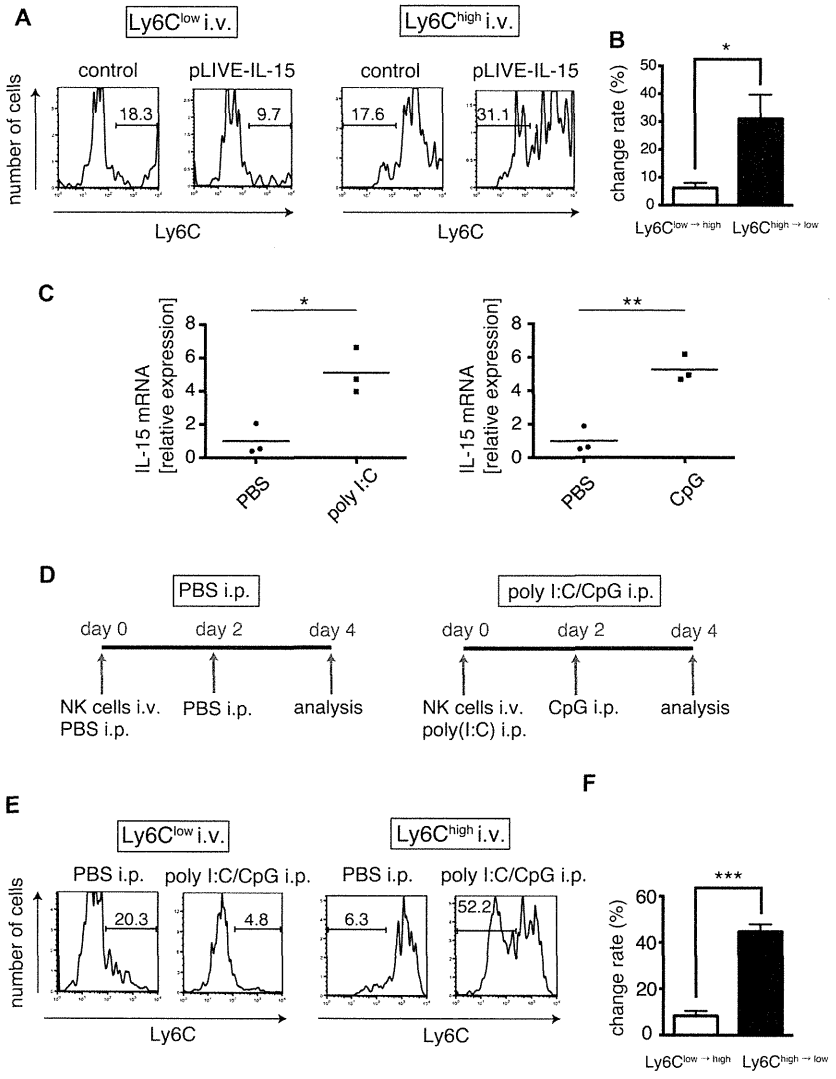

Figure 6. Conversion of Ly6C^{high} NK cells to Ly6C^{low} NK cells in vivo. (A and B) control vector or pLIVE-IL-15 (20 μg) were injected i.v. into CD45.1 congenic mice. Six hours after injection, NK-cell subsets (3×10^5 to 5×10^5cells) from the spleens of CD45.2 C57BL/6 mice were transferred into these CD45.1 mice. Four days later, cells were harvested from the spleens of the recipient mice, stained for CD49b, CD11b, CD3e, CD45.2, and Ly6C and analyzed by flow cytometry. The histogram plots show Ly6C expression profiles gated on CD49b$^+$CD11b$^+$CD3e$^-$CD45.2$^+$ cells. Numbers indicate percentages. Plots are representative of three independent experiments. (B) Change rate of each subset described in (A) (n = 4). (C) C57BL/6 mice were injected i.p. with PBS, 100 μg of polyI:C, or 20 nmol of CpG. After 3 h, splenocytes from these C57BL/6 mice were harvested. Expression of IL-15 mRNA was determined by real-time RT-PCR. The expression levels were normalized to HPRT. Each symbol represents an individual mouse and bars represent the means within the groups. Data are pooled from three independent experiments. (D) NK-cell subsets were sorted from the spleens of CD45.2 C57BL/6 mice and transferred into nonirradiated CD45.1 congenic mice. These mice were then injected i.p. with polyI:C (day 0) and CpG (day 2) or PBS (day 0 and day 2) (n = 3). Splenocytes were harvested from the recipient mice transferred with Ly6C^{low} NK cells and Ly6C^{high} NK cells. Cells were stained for CD49b, CD11b, CD3e, CD45.2, and Ly6C and assessed by flow cytometry. (E) Histograms show Ly6C expression profiles gated on CD49b$^+$CD11b$^+$CD3e$^-$CD45.2$^+$ cells. Numbers indicate percentages. (F) The graph indicates change rate of each subset in the mouse treated with both poly I:C and CpG as described in (E). Data are shown as means + SEM of three independent experiments performed. $^*p < 0.05$, $^{**}p < 0.01$, $^{***}p < 0.001$ (Student's two-tailed t-test). i.p., intraperitoneal injection, i.v., intravenous injection.

or pLIVE-IL-15 vector. Four days posttransplantation, we isolated the transferred CD45.2 NK cells from the spleen and examined their expression levels of Ly6C. Flow cytometric analysis showed that approximately 30% of the transferred Ly6C^{high} NK cells in the mouse injected with pLIVE-IL-15 were converted to Ly6C^{low} NK cells (Fig. 6A and B). In contrast, the transferred Ly6C^{high} NK cells in the mouse injected with control vector and the transferred Ly6C^{low} NK cells remained unchanged (Fig. 6A and B). We next examined the conversion during immune responses. Because DCs are known to trans-present IL-15 to NK cells when activated by viral infection or TLR ligands such as polyI:C and CpG [40–42], we evaluated the expression of IL-15 in splenocytes harvested from mice i.p. injected with polyI:C or CpG. Real-time RT-PCR analysis demonstrated that IL-15 was significantly increased in splenocytes when stimulated with polyI:C or CpG (Fig. 6C). Next, we transferred NK-cell subsets sorted from the spleens of CD45.2 C57BL/6 mice into nonirradiated CD45.1 congenic mice that had been injected i.p. with polyI:C or both polyI:C and CpG (Fig. 6D and Supporting Information Fig. 3A). Administration of both polyI:C and CpG mimics severe viral infection, and these two different TLR ligands are assumed to activate DCs synergistically [43, 44]. We then analyzed transferred NK cells in the spleen of the recipient mouse after i.p. injection of polyI:C or both polyI:C and CpG. Flow cytometric analysis indicated that approximately 30% or half of the transferred Ly6C^{high} NK cells in the mouse treated with polyI:C or both polyI:C and CpG, respectively, were converted to Ly6C^{low} NK cells (Supporting Information Fig. 3B and C and Fig. 6E and F). In contrast, the transferred Ly6C^{high} NK cells in the mouse treated with PBS and the transferred Ly6C^{low} NK cells remained unchanged (Fig. 6E and F). Collectively, these results indicate that mature NK cells can change their phenotype in response to the environment.

Discussion

In the human, mature NK cells are subdivided into two populations based on the expression levels of CD56. These two subsets, $CD56^{dim}$ and $CD56^{bright}$ NK cells, play clearly distinct roles in terms of their effector functions; that is, $CD56^{dim}$ NK cells produce low levels of IFN-γ but exhibit a high cytotoxic capacity, while $CD56^{bright}$ NK cells produce a large amount of IFN-γ but exhibit a weak cytotoxic capacity [11–13, 45]. In mice, it has been shown that mature NK cells are divided in two populations based on the CD27 expression levels and that $CD27^{low}$ NK cells are derived from $CD27^{high}$ NK cells, and exhibit lower activity than $CD27^{high}$ NK cells [14, 24]. However, the two subsets of mature NK cells in human and mouse are not the same and physiological roles of those NK subsets remain unknown. In this study, we found that mature murine NK cells are subdivided into two subsets, $Ly6C^{low}$ and $Ly6C^{high}$ NK cells, based on the expression levels of Ly6C and characterized their functions and relationship.

NK cells play major roles for host protection against infectious pathogens and tumor cells at an early stage by IFN-γ production and cytotoxicity [1, 3, 4]. We demonstrated that $Ly6C^{high}$ NK cells produced lower levels of both IFN-γ and cytotoxic granules than did $Ly6C^{low}$ NK cells, correlating with the surface phenotype of $Ly6C^{high}$ NK cells that express higher levels of inhibitory receptors. Moreover, the proliferative potential of $Ly6C^{high}$ NK cells was lower than that of $Ly6C^{low}$ NK cells when cultured with IL-15. Lower effector functions and proliferation potential suggest that $Ly6C^{high}$ NK cells are in an inert state compared with $Ly6C^{low}$ NK cells. While the frequency of $Ly6C^{high}$ NK cells in the spleen, liver, lung, and peripheral blood was almost the same, it was significantly low in the BM where NK cells derive. Moreover, adoptive transfer of each subset showed that $Ly6C^{high}$ NK cells are derived from $Ly6C^{low}$ NK cells. These results imply that $Ly6C^{high}$ NK cells in peripheral tissues are resting cells. These results are similar to the previous study showing that $CD27^{low}$ NK cells are derived from $CD27^{high}$ NK cells, and exhibit lower activity than $CD27^{high}$ NK cells [14]. However, a major finding in our study is that inert $Ly6C^{high}$ NK cells can be reactivated.

We found that $Ly6C^{high}$ NK cells can be converted to $Ly6C^{low}$ NK cells ($Ly6C^{low(high)}$ NK cells) when cultured with IL-15. The expression levels of Ly6C also decreased when cultured with IL-2, but the effect of IL-2 was not as strong as IL-15. Moreover, the ability of $Ly6C^{low(high)}$ NK cells to secrete IFN-γ and granzyme B was increased to the level comparable to that of $Ly6C^{low}$ NK cells cultured with IL-15 ($Ly6C^{low(low)}$ NK cells). This conversion of $Ly6C^{high}$ NK cells to $Ly6C^{low}$ NK cells was also shown in vivo by overexpression of IL-15 or by the administration of polyI:C and CpG, potent inducers of IL-15. These results suggest that under the steady-state conditions, $Ly6C^{low}$ NK cells with strong activity develop in the BM and become resting $Ly6C^{high}$ NK cells. However, those resting NK cells are reactivated when IL-15 expression level is increased, for example, by virus infection. Thus, the present study suggests that $Ly6C^{high}$ NK cells are a reservoir of potential NK cells that allow effective and strong response to infections.

Ly6C is known to be expressed in lymphocytes, monocytes/macrophages, granulocytes, and endothelial cells [18–20]. Although its function is not completely understood, Ly6C shows distinct expression patterns in the different developmental stages of these cells. Interestingly, naive $CD8^+$ T cells express Ly6C at low levels, but $CD8^+$ memory T cells express Ly6C at high levels [2, 20, 21]. There are many common features between NK cells and $CD8^+$ T cells [2, 22]. Both NK cells and $CD8^+$ T cells are derived from a common lymphoid progenitor, and their development and/or maintenance is regulated by IL-15. In addition, they release perforin and granzyme B in cytotoxic granules and produce a large amount of IFN-γ during viral infection or in response to proinflammatory cytokines such as IL-12. In general, $CD8^+$ memory T cells become long-lived resting cells after the first immune response and can be reactivated by encountering the same Ag [46, 47]. Considering that the functions of $Ly6C^{high}$ NK cells are suppressed in the steady state but can be reactivated by immunological stimuli, $Ly6C^{high}$ NK cells might be similar to $CD8^+$ memory T cells expressing Ly6C.

NK cells have traditionally been classified as effector cells in the innate immune system. However, a recent report showed that NK cells also possess memory function and contribute to the adaptive immune system [48, 49]. After mouse cytomegalovirus (MCMV) infection, NK cells bearing the virus-specific Ly49H receptor resided in lymphoid and nonlymphoid organs for several months [49]. These memory NK cells were reactivated, rapidly degranulated, and produced cytokines by secondary viral challenge. Interestingly, these memory NK cells showed higher expression of Ly6C. Moreover, the same group indicated that adoptive transfer of mature NK cells into lymphopenic mice resulted in the generation of long-lived NK cells [50]. These NK cells resided in both lymphoid and nonlymphoid organs for more than 6 months, retained their functionality many months after initial transfer, and responded robustly to viral infection. However, the expression levels of Ly6C of long-lived NK cells were not shown. Further studies are necessary to uncover the mechanism of differentiation of $Ly6C^{low}$ NK cells into $Ly6C^{high}$ NK cells and address whether $Ly6C^{high}$ NK cells are long-lived NK cells, memory NK cells, or their progenitors. While our results showed that different stages of NK cells are distinguishable by the Ly6C expression levels, the role of Ly6C in NK-cell function remains unknown.

In conclusion, we showed that resting $Ly6C^{high}$ NK cells are present in WT mice in the steady state, and that these $Ly6C^{high}$ NK cells can be reactivated by IL-15.

Materials and methods

Mice

WT C57BL/6J (C57BL/6) mice were purchased from CLEA Japan, Inc. CD45.1 congenic C57BL/6 mice (RBRC 00144) were provided by RIKEN BRC through the National Bio-Resource Project of the MEXT, Japan. All mice were maintained under standard

specific pathogen free (SPF) conditions and used between 10 and 14 weeks of age. The animal studies were performed according to the guidelines set by the Institutional Animal Care and Use Committee of the University of Tokyo.

Flow cytometric analysis

RBC-depleted cells were stained for the following antibodies: brilliant violet 421-conjugated anti-CD3e; FITC-conjugated anti-CD11b; PE-conjugated anti-KLRG1, Ly49H, Ly49D, Ly49A, NKG2A, NK1.1, CD45.1, and CD45.2; PE/Cy7-conjugated anti-Ly6C; biotin-conjugated anti-CD49b, CD27, NKp46, Ly108, and NKG2D; APC-conjugated streptavidin (BioLegend); PE-conjugated anti-CD3e, Ly49C/I, and Ly49F; and biotin-conjugated anti-NK1.1 (BD Pharmingen). The stained cells were analyzed using a FACS Canto II (BD Biosciences) and the FlowJo 8.8.7 software (TreeStar, Ashland, OR).

Cell culture and proliferation assay in vitro

NK cells ($CD49b^+CD11b^+CD3e^-$) were isolated from the spleens of C57BL/6 mice and further fractionated into $Ly6C^{low}$ and $Ly6C^{high}$ NK cells using a MoFlo cell sorter (Beckman Coulter). Purified $Ly6C^{low}$ and $Ly6C^{high}$ NK cells were cultured in RPMI-1640 medium containing 10% FBS, 2-ME (50 μM), HEPES (20 mM), nonessential AA, sodium pyruvate, L-Gln, and gentamycin in the presence of recombinant mouse IL-15 (100 ng/mL, eBioscience) or IL-2 (100 ng/mL, PROSPEC). Cell survival was measured in triplicate using the Trypan blue exclusion test.

ELISA

Purified murine splenic NK cells were stimulated with IL-12 (100 ng/mL, PeproTech) or IL-18 (100 ng/mL, MBL) in the presence of IL-2 (100 ng/mL, PROSPEC). After 24 h of incubation, cell-free supernatants were analyzed using an ELISA kit for IFN-γ (BD Biosciences) or granzyme B (R&D). ELISAs were performed in triplicate.

CD107a expression

NK cells ($CD49b^+$) were isolated from the spleens of C57BL/6 mice by using MACS (Miltenyi Biotec). Purified NK cells were cultured in the presence of recombinant mouse IL-2 (100 ng/mL) and IL-18 (100 ng/mL). After 16 h incubation, NK cells were stained for CD3e, CD11b, Ly6C, and CD49b. For stimulation steps, NK cells were stained for CD107a and incubated with YAC-1 cells (RCB1165 provided by RIKEN BRC through the National Bio-Resource Project of the MEXT, Japan) by an E:T ratio of 1:1 in the presence of IL-2 (100 ng/mL) and IL-18 (100 ng/mL) for 5 h at 37°C. And then, monensin solution (10 μM, BioLegend) was added during the last 4 h of the culture. Following 5 h incubation, cells were analyzed by FACS Canto II.

Adoptive cell transfer

Sorted NK cells (5×10^5 to 1×10^6 cells) from the spleens of C57BL/6 mice were injected i.v. into nonirradiated CD45.1 congenic mice. In some experiments, the mice that received NK cells were injected i.p. with polyI:C (100 μg, InvivoGen) and CpG ODN (20 nmol, Hycult Biotech) or PBS.

Overexpression by hydrodynamic tail vein injection method

Mouse IL-15 cDNA was amplified by PCR: 5′-gcgctagccacca tgaaaattttgaaaccatatatgag-3′ and 5′-cgctcgagtcaggacgtgttgatg aaca-3′, and was inserted into the NheI and XhoI sites of a pLIVE vector (Mirus, Madison, WI). pLIVE-IL-15 (20 μg) was diluted with TransIT-EE Hydrodynamic Delivery Solution (Mirus, Madison, WI) and injected i.v. into CD45.1 congenic mice. pLIVE-SEAP (secreted alkaline phosphatase) (20 μg) was used as a control [39].

Real-time RT-PCR

C57BL/6 mice were i.p. injected with PBS, polyI:C (100 μg), or CpG ODN (20 nmol). After 3 h, splenocytes from these C57BL/6 mice were harvested and total RNA was prepared using an RNeasy Mini Kit (Qiagen). The total RNA was reverse-transcribed with PrimeScript RT Master Mix (Takara Bio Ink). Quantitative real-time RT-PCR was performed on a LightCycler 480 (Roche Applied Science) using SYBR premix Ex Taq reagent (Takara Bio Ink). HPRT was used as an internal control. The sequence of primers was as follows: 5′-tctcgtgctacttgtgtttccttc-3′ and 5′-catctatccagttggcctctgtt-3′ for IL-15 and 5′-tgacactggtaaaacaat gc-3′ and 5′-tatccaacacttcgagaggt-3′ for HPRT.

Statistical analysis

Unless otherwise stated, data are shown as means ± SEM and were compared using Student's two-tailed *t*-test. A value of $p < 0.05$ was taken to indicate statistical significance. Statistical analyses were performed using GraphPad Prism (GraphPad Software, San Diego, CA).

Acknowledgments: We would like to thank Dr. Tohru Itoh for providing us with the pLIVE-SEAP vector and pLIVE-IL-15 vector.

We would also like to thanks Dr. Cindy Kok for critical reading of the manuscript. This work was supported by research grants from the Ministry of Education, Culture, Sports, Science, and Technology (MEXT) of Japan (No. 22118006), the Ministry of Health, Labour, and Welfare (MHLW) of Japan (H24-hepatitis-general-005), and the Tokyo Biochemical Research Foundation.

Conflict of interest: The authors declare no financial or commercial conflict of interest.

References

1 **Vivier, E., Tomasello, E., Baratin, M., Walzer, T. and Ugolini, S.**, Functions of natural killer cells. *Nat. Immunol.* 2008. **9**: 503–510.

2 **Sun, J. C. and Lanier, L. L.**, NK cell development, homeostasis and function: parallels with CD8(+) T cells. *Nat. Rev. Immunol.* 2011. **11**: 645–657.

3 **Cerwenka, A. and Lanier, L. L.**, Natural killer cells, viruses and cancer. *Nat. Rev. Immunol.* 2001. **1**: 41–49.

4 **Yokoyama, W. M. and Plougastel, B. F.**, Immune functions encoded by the natural killer gene complex. *Nat. Rev. Immunol.* 2003. **3**: 304–316.

5 **Spits, H., Artis, D., Colonna, M., Diefenbach, A., Di Santo, J. P., Eberl, G., Koyasu, S. et al.**, Innate lymphoid cells—a proposal for uniform nomenclature. *Nat. Rev. Immunol.* 2013. **13**: 145–149.

6 **Kim, S., Iizuka, K., Kang, H. S., Dokun, A., French, A. R., Greco, S. and Yokoyama, W. M.**, In vivo developmental stages in murine natural killer cell maturation. *Nat. Immunol.* 2002. **3**: 523–528.

7 **Strowig, T., Brilot, F. and Munz, C.**, Noncytotoxic functions of NK cells: direct pathogen restriction and assistance to adaptive immunity. *J. Immunol.* 2008. **180**: 7785–7791.

8 **Herberman, R. B., Nunn, M. E. and Lavrin, D. H.**, Natural cytotoxic reactivity of mouse lymphoid cells against syngeneic acid allogeneic tumors. I. Distribution of reactivity and specificity. *Int. J. Cancer.* 1975. **16**: 216–229.

9 **Kiessling, R., Klein, E. and Wigzell, H.**, "Natural" killer cells in the mouse. I. Cytotoxic cells with specificity for mouse Moloney leukemia cells. Specificity and distribution according to genotype. *Eur. J. Immunol.* 1975. **5**: 112–117.

10 **Lanier, L. L., Le, A. M., Phillips, J. H., Warner, N. L. and Babcock, G. F.**, Subpopulations of human natural killer cells defined by expression of the Leu-7 (HNK-1) and Leu-11 (NK-15) antigens. *J. Immunol.* 1983. **131**: 1789–1796.

11 **Frey, M., Packianathan, N. B., Fehniger, T. A., Ross, M. E., Wang, W. C., Stewart, C. C., Caligiuri, M. A. et al.**, Differential expression and function of L-selectin on CD56bright and CD56dim natural killer cell subsets. *J. Immunol.* 1998. **161**: 400–408.

12 **Jacobs, R., Hintzen, G., Kemper, A., Beul, K., Kempf, S., Behrens, G., Sykora, K. W. et al.**, $CD56^{bright}$ cells differ in their KIR repertoire and cytotoxic features from $CD56^{dim}$ NK cells. *Eur. J. Immunol.* 2001. **31**: 3121–3127.

13 **Cooper, M. A., Fehniger, T. A., Turner, S. C., Chen, K. S., Ghaheri, B. A., Ghayur, T., Carson, W. E., et al.**, Human natural killer cells: a unique innate immunoregulatory role for the CD56(bright) subset. *Blood* 2001. **97**: 3146–3151.

14 **Hayakawa, Y. and Smyth, M. J.**, CD27 dissects mature NK cells into two subsets with distinct responsiveness and migratory capacity. *J. Immunol.* 2006. **176**: 1517–1524.

15 **Huntington, N. D., Tabarias, H., Fairfax, K., Brady, J., Hayakawa, Y., Degli-Esposti, M. A., Smyth, M. J. et al.**, NK cell maturation and peripheral homeostasis is associated with *KLRG1* up-regulation. *J. Immunol.* 2007. **178**: 4764–4770.

16 **Yu, J., Wei, M., Mao, H., Zhang, J., Hughes, T., Mitsui, T., Park, I. K. et al.**, CD94 defines phenotypically and functionally distinct mouse NK cell subsets. *J. Immunol.* 2009. **183**: 4968–4974.

17 **Bamezai, A.**, Mouse Ly-6 proteins and their extended family: markers of cell differentiation and regulators of cell signaling. *Arch. Immunol. Ther. Exp. (Warsz)* 2004. **52**: 255–266.

18 **Jutila, M. A., Kroese, F. G., Jutila, K. L., Stall, A. M., Fiering, S., Herzenberg, L. A., Berg, E. L., et al.**, Ly-6C is a monocyte/macrophage and endothelial cell differentiation antigen regulated by interferon-gamma. *Eur. J. Immunol.* 1988. **18**: 1819–1826.

19 **Jutila, D. B., Kurk, S. and Jutila, M. A.**, Differences in the expression of Ly-6C on neutrophils and monocytes following PI-PLC hydrolysis and cellular activation. *Immunol. Lett.* 1994. **41**: 49–57.

20 **Hanninen, A., Maksimow, M., Alam, C., Morgan, D. J. and Jalkanen, S.**, Ly6C supports preferential homing of central memory $CD8^+$ T cells into lymph nodes. *Eur. J. Immunol.* 2011. **41**: 634–644.

21 **Walunas, T. L., Bruce, D. S., Dustin, L., Loh, D. Y. and Bluestone, J. A.**, Ly-6C is a marker of memory $CD8^+$ T cells. *J. Immunol.* 1995. **155**: 1873–1883.

22 **Bezman, N. A., Kim, C. C., Sun, J. C., Min-Oo, G., Hendricks, D. W., Kamimura, Y., Best, J. A. et al.**, Molecular definition of the identity and activation of natural killer cells. *Nat. Immunol.* 2012. **13**: 1000–1009.

23 **Sato, N., Yahata, T., Santa, K., Ohta, A., Ohmi, Y., Habu, S. and Nishimura, T.**, Functional characterization of NK1.1+Ly-6C+ cells. *Immunol. Lett.* 1996. **54**: 5–9.

24 **Chiossone, L., Chaix, J., Fuseri, N., Roth, C., Vivier, E. and Walzer, T.**, Maturation of mouse NK cells is a 4-stage developmental program. *Blood* 2009. **113**: 5488–5496.

25 **Moretta, A., Poggi, A., Pende, D., Tripodi, G., Orengo, A. M., Pella, N., Augugliaro, R. et al.**, CD69-mediated pathway of lymphocyte activation: anti-CD69 monoclonal antibodies trigger the cytolytic activity of different lymphoid effector cells with the exception of cytolytic T lymphocytes expressing T cell receptor alpha/beta. *J. Exp. Med.* 1991. **174**: 1393–1398.

26 **Falco, M., Marcenaro, E., Romeo, E., Bellora, F., Marras, D., Vely, F., Ferracci, G. et al.**, Homophilic interaction of NTBA, a member of the CD2 molecular family: induction of cytotoxicity and cytokine release in human NK cells. *Eur. J. Immunol.* 2004. **34**: 1663–1672.

27 **Flaig, R. M., Stark, S. and Watzl, C.**, Cutting edge: NTB-A activates NK cells via homophilic interaction. *J. Immunol.* 2004. **172**: 6524–6527.

28 **Nieto, M., Rodriguez-Fernandez, J. L., Navarro, F., Sancho, D., Frade, J. M., Mellado, M., Martinez, A. C. et al.**, Signaling through CD43 induces natural killer cell activation, chemokine release, and PYK-2 activation. *Blood* 1999. **94**: 2767–2777.

29 **Andrews, D. M., Scalzo, A. A., Yokoyama, W. M., Smyth, M. J. and Degli-Esposti, M. A.**, Functional interactions between dendritic cells and NK cells during viral infection. *Nat. Immunol.* 2003. **4**: 175–181.

30 **Kuribayashi, K., Gillis, S., Kern, D. E. and Henney, C. S.**, Murine NK cell cultures: effects of interleukin-2 and interferon on cell growth and cytotoxic reactivity. *J. Immunol.* 1981. **126**: 2321–2327.

31 **Meazza, R., Azzarone, B., Orengo, A. M. and Ferrini, S.**, Role of common-gamma chain cytokines in NK cell development and function: perspectives for immunotherapy. *J. Biomed. Biotechnol.* 2011. **2011**: 861920.

32 **Russell, J. H. and Ley, T. J.**, Lymphocyte-mediated cytotoxicity. *Annu. Rev. Immunol.* 2002. **20**: 323–370.

33 **Andrade, F., Roy, S., Nicholson, D., Thornberry, N., Rosen, A. and Casciola-Rosen, L.**, Granzyme B directly and efficiently cleaves several downstream caspase substrates: implications for CTL-induced apoptosis. *Immunity* 1998. **8**: 451–460.

34 **Alter, G., Malenfant, J. M. and Altfeld, M.**, CD107a as a functional marker for the identification of natural killer cell activity. *J. Immunol. Methods* 2004. **294**: 15–22.

35 **Ogasawara, K., Hida, S., Azimi, N., Tagaya, Y., Sato, T., Yokochi-Fukuda, T., Waldmann, T. A. et al.**, Requirement for IRF-1 in the microenvironment supporting development of natural killer cells. *Nature* 1998. **391**: 700–703.

36 **Kennedy, M. K., Glaccum, M., Brown, S. N., Butz, E. A., Viney, J. L., Embers, M., Matsuki, N. et al.**, Reversible defects in natural killer and memory CD8 T cell lineages in interleukin 15-deficient mice. *J. Exp. Med.* 2000. **191**: 771–780.

37 **Zhang, G., Budker, V. and Wolff, J. A.**, High levels of foreign gene expression in hepatocytes after tail vein injections of naked plasmid DNA. *Hum. Gene Ther.* 1999. **10**: 1735–1737.

38 **Zhang, G., Gao, X., Song, Y. K., Vollmer, R., Stolz, D. B., Gasiorowski, J. Z., Dean, D. A., et al.**, Hydroporation as the mechanism of hydrodynamic delivery. *Gene Ther.* 2004. **11**: 675–682.

39 **Inagaki, F. F., Tanaka, M., Inagaki, N. F., Yagai, T., Sato, Y., Sekiguchi, K., Oyaizu, N. et al.**, Nephronectin is upregulated in acute and chronic hepatitis and aggravates liver injury by recruiting CD4 positive cells. *Biochem. Biophys. Res. Commun.* 2013. **430**: 751–756.

40 **Lucas, M., Schachterle, W., Oberle, K., Aichele, P. and Diefenbach, A.**, Dendritic cells prime natural killer cells by trans-presenting interleukin 15. *Immunity* 2007. **26**: 503–517.

41 **Eidenschenk, C., Crozat, K., Krebs, P., Arens, R., Popkin, D., Arnold, C. N., Blasius, A. L. et al.**, Flt3 permits survival during infection by rendering dendritic cells competent to activate NK cells. *Proc. Natl. Acad. Sci. USA* 2010. **107**: 9759–9764.

42 **Stonier, S. W. and Schluns, K. S.**, Trans-presentation: a novel mechanism regulating IL-15 delivery and responses. *Immunol. Lett.* 2010. **127**: 85–92.

43 **Napolitani, G., Rinaldi, A., Bertoni, F., Sallusto, F. and Lanzavecchia, A.**, Selected Toll-like receptor agonist combinations synergistically trigger a T helper type 1-polarizing program in dendritic cells. *Nat. Immunol.* 2005. **6**: 769–776.

44 **Zhu, Q., Egelston, C., Vivekanandhan, A., Uematsu, S., Akira, S., Klinman, D. M., Belyakov, I. M. et al.**, Toll-like receptor ligands synergize through distinct dendritic cell pathways to induce T cell responses: implications for vaccines. *Proc. Natl. Acad. Sci. USA* 2008. **105**: 16260–16265.

45 **Caligiuri, M. A.**, Human natural killer cells. *Blood* 2008. **112**: 461–469.

46 **Kaech, S. M., Tan, J. T., Wherry, E. J., Konieczny, B. T., Surh, C. D. and Ahmed, R.**, Selective expression of the interleukin 7 receptor identifies effector CD8 T cells that give rise to long-lived memory cells. *Nat. Immunol.* 2003. **4**: 1191–1198.

47 **Wherry, E. J. and Ahmed, R.**, Memory CD8 T-cell differentiation during viral infection. *J. Virol.* 2004. **78**: 5535–5545.

48 **O'Leary, J. G., Goodarzi, M., Drayton, D. L. and von Andrian, U. H.**, T cell- and B cell-independent adaptive immunity mediated by natural killer cells. *Nat. Immunol.* 2006. **7**: 507–516.

49 **Sun, J. C., Beilke, J. N. and Lanier, L. L.**, Adaptive immune features of natural killer cells. *Nature* 2009. **457**: 557–561.

50 **Sun, J. C., Beilke, J. N., Bezman, N. A. and Lanier, L. L.**, Homeostatic proliferation generates long-lived natural killer cells that respond against viral infection. *J. Exp. Med.* 2011. **208**: 357–368.

Full correspondence: Dr. Yutaka Enomoto, Laboratory of Cell Growth and Differentiation, Institute of Molecular and Cellular Biosciences, The University of Tokyo, 1-1-1 Yayoi, Bunkyo-ku, Tokyo 113-0032, Japan
Fax: +81-3-5841-8475
e-mail: yenomoto@iam.u-tokyo.ac.jp

Additional correspondence: Dr. Atsushi Miyajima, Laboratory of Cell Growth and Differentiation, Institute of Molecular and Cellular Biosciences, The University of Tokyo; 1-1-1 Yayoi, Bunkyo-ku, Tokyo 113-0032, Japan
e-mail: miyajima@iam.u-tokyo.ac.jp

Received: 16/2/2014
Revised: 9/6/2014
Accepted: 1/7/2014
Accepted article online: 3/7/2014

PLOS | ONE

RESEARCH ARTICLE

Oncostatin M Maintains the Hematopoietic Microenvironment in the Bone Marrow by Modulating Adipogenesis and Osteogenesis

Fumi Sato[1], Yuichiro Miyaoka[1¤], Atsushi Miyajima[1], Minoru Tanaka[2,3*]

1. Laboratory of Cell Growth and Differentiation, Institute of Molecular and Cellular Biosciences, The University of Tokyo, Tokyo, Japan, **2.** Laboratory of Stem Cell Regulation, Institute of Molecular and Cellular Biosciences, The University of Tokyo, Tokyo, Japan, **3.** Department of Regenerative Medicine, Research Institute, National Center for Global Health and Medicine, Tokyo, Japan

*tanaka@iam.u-tokyo.ac.jp

¤ Current address: Gladstone Institute of Cardiovascular Disease, San Francisco, California, United States of America

OPEN ACCESS

Citation: Sato F, Miyaoka Y, Miyajima A, Tanaka M (2014) Oncostatin M Maintains the Hematopoietic Microenvironment in the Bone Marrow by Modulating Adipogenesis and Osteogenesis. PLoS ONE 9(12): e116209. doi:10.1371/journal.pone.0116209

Editor: Hiroyasu Nakano, Toho University School of Medicine, Japan

Received: June 17, 2014

Accepted: December 4, 2014

Published: December 31, 2014

Data Availability: The authors confirm that all data underlying the findings are fully available without restriction. All relevant data are within the paper and its Supporting Information files.

Funding: This work was supported by Grants-in-Aid for Scientific Research on Innovative Areas 22118006 from the Japan Society for the Promotion of Science, Japan. The funders had no role in study design, data collection and analysis, decision to publish, or preparation of the manuscript.

Competing Interests: The authors have declared that no competing interests exist.

Abstract

The bone marrow (BM) is an essential organ for hematopoiesis in adult, in which proliferation and differentiation of hematopoietic stem/progenitor cells (HSPC) is orchestrated by various stromal cells. Alterations of BM hematopoietic environment lead to various hematopoietic disorders as exemplified by the linking of fatty marrow with increased adipogenesis to anemia or pancytopenia. Therefore, the composition of mesenchymal stromal cell (MSC)-derived cells in the BM could be crucial for proper hematopoiesis, but the mechanisms underlying the MSC differentiation for hematopoiesis remain poorly understood. In this study, we show that Oncostatin M (OSM) knock out mice exhibited pancytopenia advancing fatty marrow with age. OSM strongly inhibited adipogenesis from BM MSC *in vitro*, whereas it enhanced their osteogenesis but suppressed the terminal differentiation. Intriguingly, OSM allowed the MSC-derived cells to support the *ex vivo* expansion of HSPC effectively as feeder cells. Furthermore, the administration of OSM in lethally irradiated wild-type mice blocked fatty marrow and enhanced the recovery of HSPC number in the BM and peripheral blood cells after engraftment of HSPC. Collectively, OSM plays multiple critical roles in the maintenance and development of the hematopoietic microenvironment in the BM at a steady state as well as after injury.

Introduction

The bone marrow (BM) is a major tissue that supplies blood throughout life. Hematopoietic stem cells (HSC) are surrounded by various types of stromal cells and the proliferation and differentiation of HSC is tightly regulated in the BM microenvironment [1]. Two types of functional niches for supporting HSC in the BM have been studied; i.e., the osteoblastic niche [2–4] and perivascular niche [5–7], which are composed of osteoblasts and endothelial cells/perivascular mesenchymal cells, respectively. Mesenchymal stromal cells (MSC) in the BM can give rise to multiple cell lineages *in vitro*, including adipocytes, osteocytes, and chondrocytes [8, 9]. Recently, it has been reported that a subset of MSC (PDGFα+Sca-1+CD45-TER119-; PαS cell) in the BM could differentiate into hematopoietic niche cells, osteoblasts, and adipocytes after *in vivo* transplantation [10], although it remains to be elucidated whether the PαS-derived cells function as HSPC niche in the BM and what factors regulate the differentiation of PαS cell *in vivo*.

On the other hand, Naveiras et al. reported the BM adipocytes as negative regulators of the hematopoietic microenvironment using lipoatrophic A-ZIP/F1 'fatless' mice [11]. In the study, transplantation of normal BM cells in lethally irradiated A-ZIP/F1 mice lacking adipogenesis showed enhanced hematopoietic recovery compared with wild-type recipient mice, indicating that adipocytes in fatty marrow hinder hematopoietic progenitor expansion. In humans, it is also known that fatty marrow gradually predominates with age [12]. It should be noted that some myeloid diseases such as aplastic anemia (AA) displaying anemia, and/or pancytopenia are accompanied by severe fatty marrow [13]. These reports strongly suggest that the cellularity of adipocytes, osteoblasts and other mesenchymal stromal cells in the BM is critical for an adequate hematopoietic microenvironment. As these cells could be derived from MSC in the BM, the factor(s) that regulate their balance would be a novel therapeutic target for impaired hematopoiesis in fatty marrow and for enhancing hematopoietic engraftment after BM transplantation.

OSM is a member of the interleukin (IL)-6 family of cytokines and has various unique biological activities e.g. hematopoiesis, hepatogenesis and adipogenesis, which are not shared by the other family members [14]. Murine OSM is expressed in the aorta-gonad-mesonephros (AGM) region, where long-term repopulating HSC (LT-HSC) arise, and OSM stimulates the expansion of multipotential hematopoietic progenitors in the primary culture of AGM [15]. While OSM also expanded hematopoietic stem/progenitor cells (HSPC) in co-cultures of AGM and fetal liver cells [16], it induced the differentiation of fetal hepatocytes *in vitro* [17]. Despite its strong and unique activities *in vitro*, the genetic ablation of either OSM or its receptor (OSMR) in mice unexpectedly showed no severe defects during development [18, 19]. In contrast, these adult knockout (KO) mice displayed anemic and thrombocytopenic phenotype although the symptoms were relatively mild. Colony-forming unit (CFU) assays showed that the number of hematopoietic progenitors in BM was significantly reduced in KO mice compared

to wild-type (WT) mice, whereas that in spleen was increased. Additionally, the number of hematopoietic progenitors in peripheral blood was increased in OSM KO mice, indicating the mobilization of HSPC from the BM into the circulation. These reports suggest the possibility that the BM niche harboring HSPC is impaired in OSM KO mice.

OSM was shown to inhibit the adipocytic differentiation of 3T3L1 cells, a preadipocyte cell line, mouse embryonic fibroblasts (MEFs), adipose tissue-derived MSC and BM MSC [20–22]. Considering the BM adipocytes as a negative regulator of the hematopoietic microenvironment [11], the lack of inhibitory effect of OSM on adipogenesis from MSC may account for the reduced hematopoietic activity in OSM KO BM. However, the causal linkage between these two original findings has remained uninvestigated. Although Walker et al. reported that marrow adipocyte volume was increased in 12-week-old OSMR KO mice [22], the role of OSM in the BM microenvironment for hematopoiesis has not been elucidated. By contrast, several reports have demonstrated that OSM induces osteogenic differentiation of human MSC and a murine stromal cell line [21–23], suggesting a role for OSM in the hematopoietic microenvironment.

In this report, we aimed to unravel the roles of OSM in the BM hematopoietic microenvironment under various conditions, BM injuries by chemicals or irradiation and aging. In addition, we prepared PαS MSC from WT and OSMR KO BM to examine the biological activities of OSM in their adipogenic and osteogenic differentiation and evaluated the hematopoietic capacity by developing a co-culture system with HSPC. We further present the possibility to use OSM as a promising therapeutic agent to enhance the recovery of hematopoiesis after BM lesion. Our results demonstrate that OSM contributes to the maintenance of the hematopoietic microenvironment by balancing multiple steps of differentiation of BM MSC in both steady and injured states.

Materials and Methods

Mice

C57BL/6J mice were purchased from Clea Japan, Inc. (Tokyo, Japan). CD45.1 (C57BL/6) congenic mice were also purchased from the RIKEN Research Center. OSM KO mice and OSMR KO mice were generated as described previously [18, 19]. All animals were maintained in a standard Specific-Pathogen Free (SPF) room at our animal facility. All animal experiments were performed according to the guidelines approved by the Institutional Animal Care and Use Committee of the University of Tokyo.

Surgical and chemical treatment

For splenectomy, the spleen was removed surgically from anesthetized 10-week-old mice after the splenic artery was ligated by 4-0″ suture (Vicryl; Ethicon, Inc., Somerville, NJ, USA). For myeloablation, 10 mg of busulfan (Sigma-Aldrich, St.

Louis, MO, USA) were dissolved in 1 mL of acetone (Wako Chemical Co., Kyoto, Japan), and then 4 mL of sterilized distilled water were added to yield a final concentration of 2 mg/mL. Next, 20 mg/kg of busulfan was administered intraperitoneally three times over a 1-week period. Mice were sacrificed 1 week after the final administration.

Measurement of hematocrit values and plasma Erythropoietin (EPO) levels

Peripheral blood was placed into heparinized Micro-Hematocrit Capillary tubes (Thermo Fisher Scientific, Waltham, MA, USA) and centrifuged at 3000 rpm for 20 min at room temperature. After determining the hematocrit value, the plasma was collected for measurement of the plasma EPO concentration. The plasma EPO concentration was measured using a mouse EPO ELISA kit as described in the manufacturer's protocol (R&D Systems, Minneapolis, MN, USA).

Preparation of BM sections

The femurs were excited and immersion-fixed in 10% neutral-buffered formalin, pH 7.0–7.5 (Wako) at 4℃ for 24 h. After washing under gently running water, the femurs were demineralized at 4℃ for 12 days in decalcifying Solution B (0.5 M EDTA, pH 7.4) (Wako). For Oil Red O staining, demineralized femurs were immersed sequentially in 5, 10, 15, and 20% sucrose-phosphate-buffered saline (PBS) for 6 h each. Finally, the femurs were embedded in OCT compound (Sakura Finetek Inc., Torrance, CA, USA) and sliced into 14-μm sections using a cryostat (MICROM HM 525; Thermo Fisher Scientific).

Isolation of PαS cells from adult mouse BM

PαS cells, which co-expressed PDGFRα and Sca-1, but not CD45 and TER119, were isolated from the bone of WT or OSMR KO mice as described by Morikawa et al. [10]. Briefly, bone marrow was flushed out from femurs and tibias of 8–12 mice using 22- and 23-G needles (Terumo) and the remaining bone was ground with a pestle. Then, the crushed bone fragments were treated with 0.2% collagenase (Sigma) for 30 min at 37℃. Next, after depletion of mature red blood cells using hypotonic lysis buffer (0.38% NH_4Cl) for 7 min on ice, the cells were incubated with anti-FcR for 15 min on ice. The cells were then incubated with allophycocyanin (APC)-conjugated rat anti-mouse PDGFRα (APA5; eBioscience, San Diego, CA, USA), fluorescein isothiocyanate (FITC)-conjugated rat anti-mouse Sca-1 (E13-161.7; BD Biosciences, Franklin Lakes, NJ, USA), phycoerythrin (PE)-conjugated rat anti-mouse CD45 (30-F11; BD Biosciences), and PE-conjugated rat anti-mouse TER119 (TER-119; eBioscience). After dead cells were excluded by propidium iodide staining, the $CD45^-$ $TER119^-$ $PDGFR\alpha^+$ $Sca\text{-}1^+$ cells were sorted using a Moflo XDP cell sorter (Beckman-Coulter, Fullerton, CA, USA). MSC were sub-cultured in α-MEM (Invitrogen, Carlsbad, CA, USA)

supplemented with 10% fetal bovine serum (JRH Biosciences, Inc., Lenexa, KS, USA), penicillin-streptomycin-glutamine solution (Invitrogen), and Gluta-Max (Invitrogen).

Adipogenic differentiation assay

Adipocyte differentiation of PαS cells was performed using Adipogenic Induction Medium/Adipogenic Maintenance Medium (Lonza, Walkersville, MD, USA) and supplements from the Adipogenic Induction/Adipogenic SingleQuots Kit (Lonza), according to the manufacturer's protocol. Briefly, PαS cells were seeded at 10,000/well into six-well plates (Corning Inc., Corning, NY USA) and allowed to reach sub-confluence. Next, PαS cells were cultured with three cycles of Adipogenic Induction Medium/Adipogenic Maintenance Medium. OSM was added to only the Adipogenic Induction Medium. Oil Red O staining was performed as described previously [20].

Osteogenic differentiation assay

Osteogenic differentiation of the PαS cells was performed using Osteogenic Induction Medium (Lonza) and supplements from the Osteogenic SingleQuots Kit (Lonza), according to the manufacturer's protocol. Briefly, PαS cells were seeded at 30,000/well in maintenance medium and allowed to attach. Next, the medium was changed to the osteogenic induction medium in the presence or absence of OSM. Alizarin Red S staining was used to evaluate osteoblastic differentiation by detecting mineralized nodules. Alizarin Red S (Sigma) was dissolved in distilled water, and the pH was adjusted to pH 6.38 by the addition of 0.25% ammonium hydroxide. Cultured cells were washed with PBS and fixed in 95% ethanol for 10 min at room temperature. After washing with distilled water, the cells were incubated in Alizarin Red S solution for 10 min at room temperature. The cells were then gently washed with distilled water, 95% and 100% ethanol.

Real-time RT-PCR analyses

Total RNA was collected from the BM, spleen, and liver of WT or OSM KO mice using TRIzol reagent, according to the manufacturer's instructions (Invitrogen). After treatment with DNase I (Invitrogen), total RNA was reverse-transcribed using the Prime Script RT Reagent Kit (TaKaRa, Shiga, Japan) and subjected to real-time PCR analyses using a Light Cycler 480 (Roche, Mannheim, Germany). For adipogenic and osteogenic differentiation assays, real-time RT-PCR was performed as above. Data were normalized to beta-actin expression. Primer sequences are shown in S1 Table.

Preparation of LSK cells from adult mouse BM

Single-cell suspensions of whole BM cells were labeled by incubation on ice for 15 min using a cocktail of the following antibodies: PE-conjugated anti-mouse CD3ε (145-2C11; BD Biosciences), CD4 (L3T4; BD Biosciences), CD8α (53-6.7; BD Biosciences), B220 (RA3-6B2; BD Biosciences), Mac-1 (M1/70; BD Biosciences), Gr-1 (RB6-8C5; eBioscience), and Ter119 (TER-119, eBioscience); FITC-conjugated anti-mouse Sca-1 (E13-161.7; BD Biosciences); and APC-conjugated anti-mouse c-Kit (2B8; BD Biosciences). After cells were washed with PBS, they were incubated with anti-PE microbeads (Miltenyi Biotec, Bergisch Gladbach, Germany) at 4℃ for 15 min. Lin^+ cells ($CD4^+$, $CD8\alpha^+$, $B220^+$, $Mac\text{-}1^+$, $Gr\text{-}1^+$, $Ter119^+$ cells) were removed by immunomagnetic selection using a MACS system (Miltenyi Biotec). These negatively selected cells were subjected to FACS using a Moflo XDP cell sorter (Beckman-Coulter) to prepare LSK cells.

Co-culture system

The co-culture system was developed by modifying the HSC expansion system [24]. WT-PαS cells were freshly sorted by FACS and plated at 2000/well in a 96-well plate (Corning Inc.). After PαS cells were cultured in maintenance medium until sub-confluent growth, the medium was changed to osteogenic induction medium in the presence or absence of OSM. At day 7 of osteogenic induction, the medium was removed, rinsed, and replaced with 200 μl of HSC culture medium containing 5,000 LSK cells. The HSC culture medium consists of StemSpan SFEM medium (Stemcell Technologies, Inc., Vancouver, British Columbia, Canada) supplemented with 50× penicillin/streptomycin (Life Technologies, Carlsbad, CA, USA), 10 ng/mL recombinant mouse SCF (Pepro Tech, Inc., Rocky Hill, NJ, USA). After co-culture, cells were inoculated at 37℃ under 4% O_2 and 5% CO_2 conditions for 7 days. One hundred microliters of medium were replaced with fresh HSC culture medium every 2–3 days. At day 7 of co-culture, after treatment with 0.25% trypsin-EDTA, nucleated cells were enumerated using a hemocytometer after staining with Turk's solution (Wako). Re-analyses of the LSK fraction in expanded cells were performed using the BD FACS Canto II system (BD Biosciences). Data were analyzed using the FlowJo software.

Irradiation and OSM administration

CD45.2 recipient mice were exposed to lethal dose of radiation (M-150WE; Softex) and BM cells prepared from CD45.1 donor mice were injected intravenously. Primary administration of OSM was performed in conjunction with BM transplantation at a dose of 600 ng per a mouse. Then, OSM was administrated intraperitoneally twice (10 a.m. and 6 p.m.) a day for 7 days. Mice were sacrificed at day 7 after irradiation, and the BM of femurs was analyzed by Oil red O staining and real-time RT-PCR. Blood was collected from a tail vein every 7 days during the recovery process, and analyzed by using an automated counter pocH-100iV (Sysmex).

Statistical methods

Differences between means were evaluated using a standard unpaired, one-way Student's t-test. Data were indicated as the means ± standard deviation (S.D.) or standard error of the mean (S.E.M.). A value of $p<0.05$ was taken to indicate statistical significance.

Results

Impaired hematopoietic activity of OSM-deficient BM

We have reported previously that OSM KO and OSMR KO mice exhibit mild anemic and thrombocytopenic phenotype, whereas the count of white blood cells in peripheral blood is normal [18, 19]. The hematopoietic activity in the BM of both types of KO mice evaluated by CFU assays was significantly lower than that in WT mice. Conversely, both types of KO mice showed an increase in hematopoietic activity in the spleen, compensating for the reduced hematopoiesis in the BM by the extramedullary hematopoiesis. To focus on the hematopoiesis in the BM, we performed splenectomy (Spx) and monitored the hematocrit (HCT), the volume percentage of red blood cells in peripheral blood. The Spx-treated WT mice showed a normal HCT value of ~50% 1 week after surgery, which was maintained thereafter up to 8 weeks. By contrast, the HCT value of the Spx-treated OSM KO mice fell to ~40% 1 week later. Interestingly, it showed no sign of recovery from anemia for 8 weeks (Fig. 1A). Erythropoietin (EPO) is a critical factor required for erythroid development and contributes to the optimal tissue oxygenation by regulating the number of peripheral erythrocytes [25]. To investigate whether the anemia in Spx-treated OSM KO mice is caused by insufficient EPO production, we measured the EPO concentration in plasma by enzyme-linked immunosorbent assay (ELISA). In WT mice, the concentration of serum EPO increased significantly by 3.9-fold after 1 week of Spx treatment (Fig. 1B), and the HCT value returned to the normal level, indicating that the kidney adequately upregulated EPO expression by sensing the hypoxic condition. Similarly, the serum EPO level of OSM KO mice increased by 2.1-fold after 1 week of Spx treatment, suggesting that the sensor for hypoxia functions normally in OSM KO mice. Despite the increase in EPO, however, the HCT values of OSM KO mice were not recovered for at least 8 weeks. Additionally, even in the steady-state condition before Spx, the serum EPO level in OSM KO mice was 2.8-fold higher than that in WT mice, suggesting that the OSM KO BM could not fully support erythropoiesis irrespective of the presence of excess EPO. These results indicate an abnormality in the BM microenvironment for hematopoietic progenitor cells in OSM KO mice.

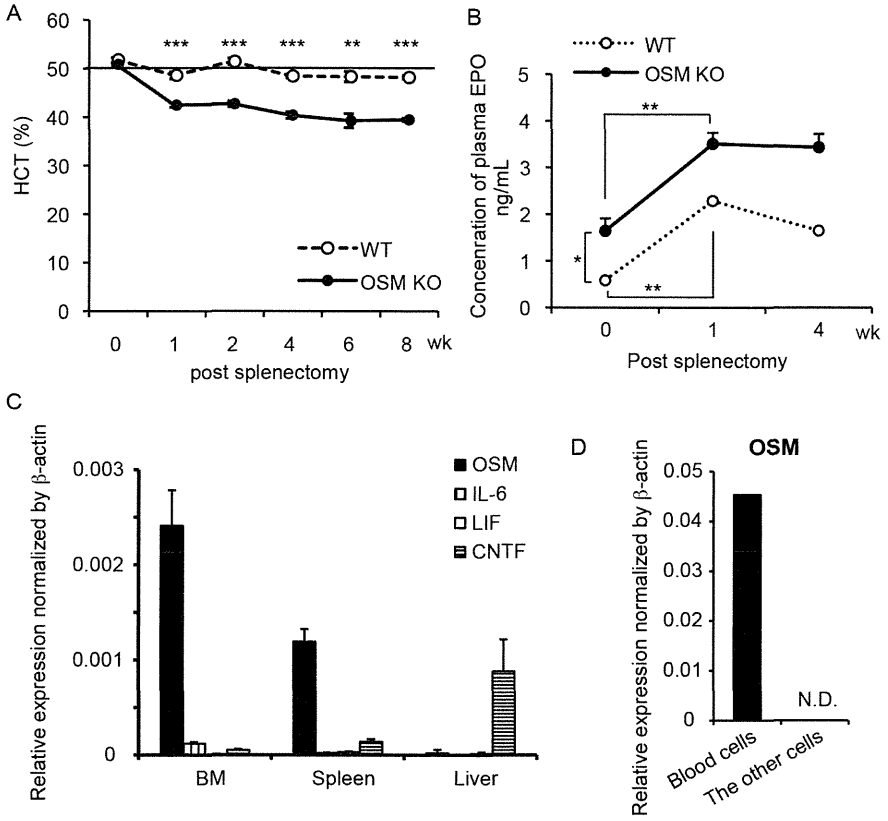

Fig. 1. Impaired BM hematopoiesis in OSM KO mice. (A) Hematocrit values of WT (dashed line) and OSM KO mice (solid line) after Spx treatment. Hematocrit values in Spx-treated OSM KO mice showed no sign of recovery from anemic symptoms. Data are presented as means ± S.E.M. (n=4). (B) Plasma concentrations of EPO in WT (dashed line) and OSM KO mice (solid line) by ELISA. Data are presented as means ± S.E.M. (n=4). (C) Gene expression analysis of IL-6 family cytokines (OSM, IL-6, LIF, and CNTF) in the BM of WT mice. The expression level was normalized against that of β-actin. Data are presented as means ± S.D. (n=4). (D) Real-time RT-PCR analysis of OSM mRNA expression in $CD45^+$ $Ter119^+$ cells (blood cells) and $CD45^-Ter119^-$ cells (the other cells) of the BM. *P<0.05, **P<0.01, ***P<0.001. N.D., not detected.

doi:10.1371/journal.pone.0116209.g001

OSM is predominantly and constitutively expressed in the BM among IL-6 family cytokines

Because IL-6 family cytokines are known to exhibit similar activity via the shared receptor subunit gp130 [14], we examined the expression profile of IL-6 family cytokines in the BM, spleen, and liver. The expression levels of mRNA for OSM, IL-6, leukemia inhibitory factor (LIF), and ciliary neurotrophic factor (CNTF) relative to β-actin were measured by real-time reverse transcription-polymerase chain reaction (RT-PCR) (Fig. 1C). OSM was highly expressed in both the BM and spleen as previously reported, but not in the liver [26]. Compared to OSM, levels of the other cytokines in the BM were negligible, indicating that, among the IL-6 family cytokines, OSM is predominantly and constitutively expressed in the BM. Furthermore, we subdivided BM cells into blood ($CD45^+$ and $TER19^+$ cells) and the other cells by fluorescence-activated cell sorting (FACS) to identify the

OSM-producing cells in the BM (Fig. 1D). Real-time RT-PCR revealed that hematopoietic cells were the major source of OSM regardless of inflammation, while OSM has been reported to be induced by activated macrophages and T-cells [27, 28]. Thus, the expression profile of OSM supports the idea that OSM contributes largely to the maintenance of the BM microenvironment, consistent with our previous report that the transplantation of WT BM cells into OSMR KO mice failed to recover the activity of hematopoietic progenitor cells in the recipient BM [19].

Fatty marrow is exaggerated with age as well as by myeloablation in OSM KO mice

Because the BM adipocytes are considered to negatively affect the hematopoietic microenvironment [11], we hypothesized that the adipogenic property of OSM KO BM contributed to the impairment of hematopoietic niche. In humans and mice, it is known that the number of adipocytes in the BM increases spontaneously with age [12, 29]. To investigate whether aging accelerates the accumulation of lipid in BM of OSM KO mice, we performed Oil Red O staining of young and aged WT and OSM KO femurs. The BM of young (10-week-old) and aged (32-week-old) OSM KO mice showed mild and massive accumulation of lipid, respectively, while those of WT mice showed little staining (Fig. 2A). Consistently, the real-time RT-PCR analysis of adipogenesis-related gene expression in the BM revealed a significant increase of perilipin, which is known to be involved in the formation of lipid droplets [30, 31], in the BM of aged OSM KO mice (Fig. 2B). These results suggested that OSM is involved in the alteration of BM cellularity with ageing and that the adipogenic property and lipid accumulation in the OSM KO BM contributes to impaired hematopoietic niche in aged mice. Therefore, we analyzed the peripheral blood of 40-week-old WT and OSM KO mice (Table 1). The count of peripheral red blood cells (RBC) and platelets (PLT) in the aged OSM KO mice exhibited significant anemic and thrombocytopenic phenotypes compared to WT mice, while those phenotypes in young adult OSMR KO mice were relatively mild as reported previously [19]. In addition, the aged OSM KO mice showed marked reduction of peripheral white blood cells (WBC) number compared to WT mice, which was not observed in young adult OSMR KO [19]. These results suggested that the lack of OSM in the BM could promote fatty marrow with age, leading to pancytopenia.

Given that the massive accumulation of BM adipocytes in the aged OSM KO mice results from stromal cell turnover, the regenerative process of the BM microenvironment after BM lesion may elicit the adipogenesis even in young mice. Based on this idea, mice were administered with busulfan, an alkylating antineoplastic agent known to induce myeloablation of BM stromal cells as well as hematopoietic cells [32]. We injected busulfan into Spx-treated WT and OSM KO mice three times every other week to induce the reconstruction of the BM microenvironment, and then evaluated the adipogenic status in the BM 7 days after the final injection (Fig. 2C). Expectedly, marked accumulation of lipid was

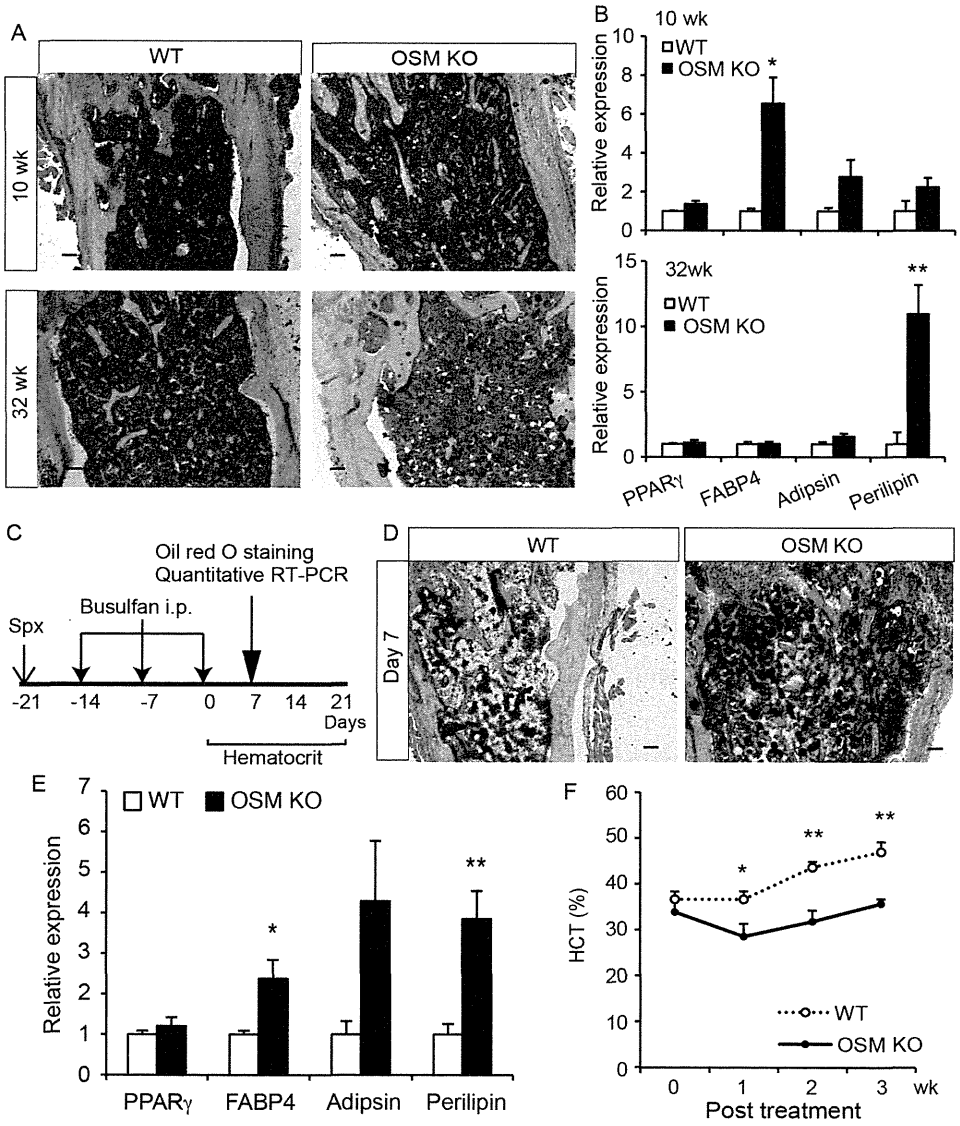

Fig. 2. Adipogenic BM of OSM KO mice by aging and injury. (A) Oil Red O staining of femurs of young (10-week-old) and aged (32-week-old) WT and OSM KO mice (14-μm frozen sections). (B) Expression of adipogenesis-related genes by real-time RT-PCR in the BM of 10- and 32-weeks-old WT and OSM KO mice (n=5). (C) The experimental design of chemotherapy-induced myeloablation. WT and OSM KO mice were splenectomized and then treated with an intraperitoneal injection of 20 mg/kg busulfan three times. After the final injection the hematocrit value was monitored weekly for 3 weeks. (D) Oil Red O staining of femur sections from WT and OSM KO mice 7 days after myeloablation. (E) Real-time RT-PCR analyses of the genes related to adipogenesis. The expression levels of adipsin and perilipin mRNA are shown (n=4). (F) Hematocrit values after busulfan treatment of WT (open circle) and OSM KO mice (closed circle) (WT: 0–7 days, n=8; 14–21 days, n=3; OSM KO: 0–7 days, n=5; 14–21 wks, n=3). Data are shown as means ± S.E.M. *P<0.05, **P<0.01. Scale bars indicate 100 μm.

doi:10.1371/journal.pone.0116209.g002

observed in OSM KO BM compared with WT BM by Oil Red O staining (Fig. 2D). Consistently, the expression of perilipin was strikingly upregulated in OSM KO BM during the reconstruction of the BM (Fig. 2E), indicating that myeloablation triggered severe fatty marrow in OSM KO mice. In addition, we

Table 1. Hematologic analysis of the peripheral blood of 40-weeks-old mice.

	Unit	WT	OSM KO
RBC	x 10^6/μL	9.37±0.15	7.41±0.14***
PLT	x 10^6/μL	1.3±0.05	0.7±0.03***
HCT	%	49.8±1.53	39.6±0.64***
HGB	g/dL	14.1±0.24	12.4±0.18***
WBC	x 10^3/μL	8.38±0.79	2.79±0.22***
Rtc	‰	32.5±1.06	27.1±1.39**
MCV	fL	52.7±0.62	53.7±0.46

RBC, red blood cells; PLT, platelets; HCT, hematocrit value; HGB, hemoglobin; WBC, white blood cells. Rtc, reticulocyte; MCV, mean corpuscular volume.
**P<0.01,
***P<0.001, WT, n=6; OSM KO, n=7.
Deta represent mean ± SEM.

doi:10.1371/journal.pone.0116209.t001

monitored the HCT value in peripheral blood every week. While the HCT value in WT mice returned to the normal level 3 weeks after the final busulfan injection, the recovery of HCT value in OSM KO mice was blunted (Fig. 2F). These results strongly suggested that OSM plays a role in the development and maintenance of the BM microenvironment.

OSM directly inhibits adipocytic differentiation of BM MSC *in vitro*

Recently, Morikawa et al. reported that a subset of MSC, so-called PαS cells in the BM, could differentiate into hematopoietic niche cells, osteoblasts and adipocytes after transplantation *in vivo* [10]. They also demonstrated the differentiation potentials of PαS cells *in vitro* into three distinct cell lineages; i.e., osteocytes, adipocytes, and chondrocytes. Therefore, we investigated whether OSM could inhibit the adipocytic differentiation of PαS cells *in vitro*. At first, we isolated PαS cells from femurs of either WT or OSMR KO mice by cell sorting, as reported previously, and named them "WT-PαS cells" and "OSMR KO-PαS cells", respectively. As shown in S1 Fig., little difference was found between the percentages of WT-PαS cells and OSMR KO-PαS cells in BM non-hematopoietic cells. Additionally, cultured WT-PαS cells and OSMR KO-PαS cells exhibited no apparent difference in their spindle morphology in the maintenance medium culture (S1 Fig.). It is, therefore, likely that the number and characteristics of PαS cells in WT and OSMR KO BM are comparable regardless of OSM signaling *in vivo*. To examine the inhibitory effect of OSM on adipocytic differentiation of PαS cells *in vitro*, we induced adipogenesis in the presence or absence of OSM. After adipogenic induction, both WT-PαS and OSMR KO-PαS cells accumulated lipid in the absence of OSM as evaluated by Oil red O staining (Fig. 3A). By contrast, in the presence of OSM, the adipogenesis of WT-PαS was completely blocked, and the inhibitory effect was canceled in OSMR KO-PαS due to the lack of the OSM receptor. In line with that observation, the expression of fat-related genes, adipsin and perilipin were markedly downregulated by the addition of OSM in WT-PαS

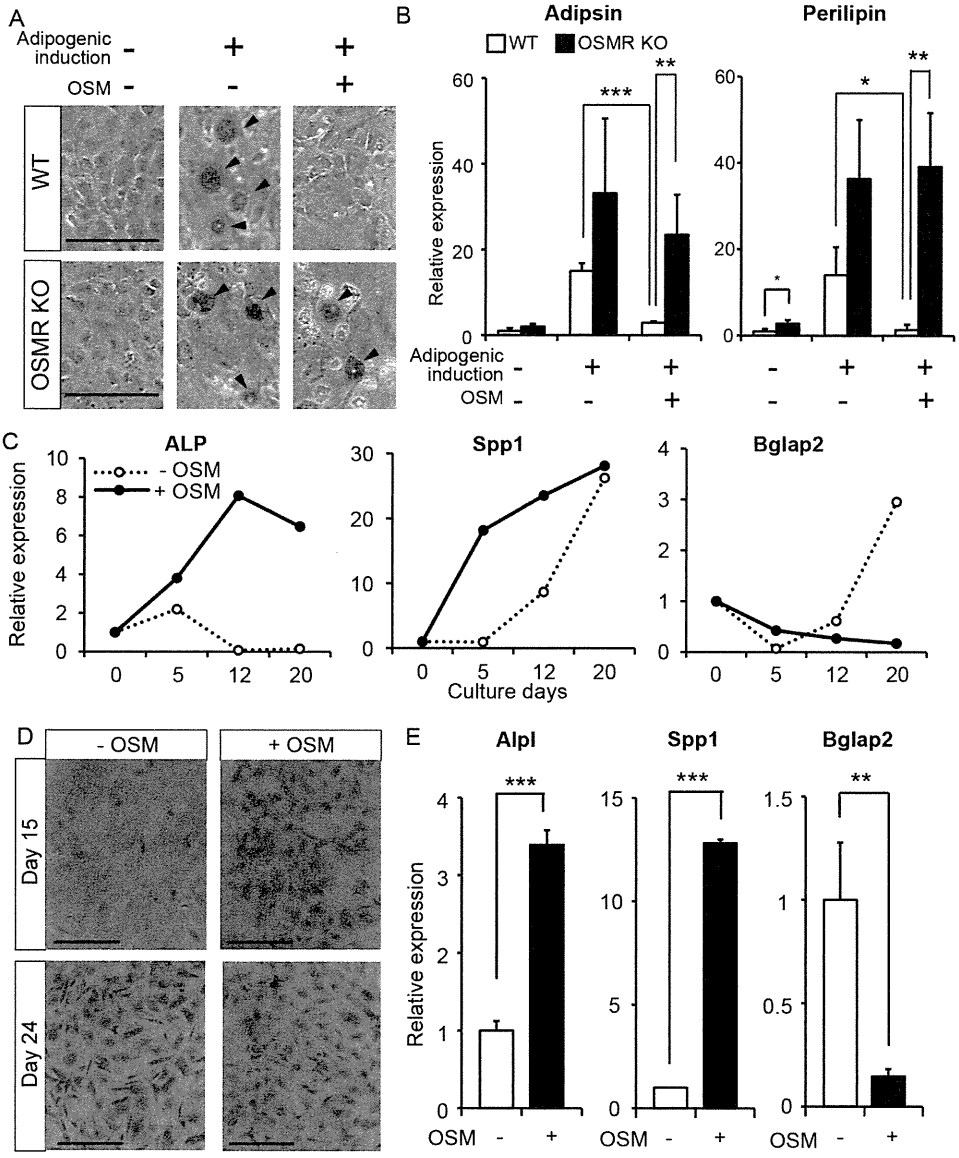

Fig. 3. Multiple roles of OSM in differentiation of PαS cells *in vitro*. (A) Evaluation of lipid accumulation in the cells by Oil Red O staining. Adipocytic-differentiated cells are indicated by arrowheads. (B) Real-time RT-PCR analysis of genes related to adipocytic differentiation. The expression levels of adipsin, and perilipin mRNA are shown (n=4). (C) The expression profiles of osteogenesis-related genes after induction of osteogenic differentiation. The expression levels of Alpl, Spp1 and Bglap2 were measured by real-time RT-PCR after 5, 12, and 20 days of osteogenic induction in the presence (closed circle) or absence (open circle) of 10 ng/mL OSM. (D) Alizarin Red S staining after 15 days and 24 days of induction. (E) Real-time RT-PCR analysis of Alpl, Spp1 and Bglap2 after 7 days of culture with Dex (n=3). Data are presented as means ± S.D. *P<0.05, **P<0.01, ***P<0.001. Scale bars indicate 100 μm.

doi:10.1371/journal.pone.0116209.g003

cell culture but not in OSMR KO-PαS cell culture (Fig. 3B). These results clearly indicated that OSM strongly inhibits the adipocytic differentiation of PαS cells *in vitro*.

OSM accelerates osteogenic differentiation of PαS cells but suppresses their terminal differentiation *in vitro*

The finding that OSM strongly inhibited the adipocytic differentiation of PαS cells raised the possibility that OSM contributes to the hematopoietic microenvironment by biasing PαS cells towards the other type of mesenchymal stromal cell. OSM may rather enhance the osteogenic differentiation of PαS cells directly as reported in previous works using other BM MSC [22, 23]. To address the possibility, we evaluated osteogenic differentiation in WT-PαS cell culture with or without OSM. It is known that alkaline phosphatase (Alpl), secreted phosphoprotein 1 (Spp1) and bone gamma-carboxyglutamate protein 2 (Bglap2) (also known as osteopontin and osteocalcin, respectively) are expressed in osteocytic cells and that a cascade of gene induction occurs concomitantly with osteoblastic differentiation [33]. In short, Alpl is an early marker of osteogenic differentiation, but its expression decreases toward terminal differentiation. Spp1 is subsequently upregulated, and finally Bglap2 is induced and maintained in terminally differentiated osteocytes. The osteogenic differentiation of PαS induced the sequential expression of Alpl, Spp1, and Bglap2 along with osteogenesis in the absence of OSM (Fig. 3C). By contrast, the addition of OSM induced Alpl and Spp1 strongly even at the early stage of osteogenic differentiation (day 5 and day 12). Consistently, Alizarin red S staining, which reflects the extent of mineralization in the cells, demonstrated that positively stained cells appeared in the presence of OSM earlier than in the absence of OSM (Fig. 3D). These results suggested that OSM accelerates the osteogenic differentiation of PαS cells as is the case with other works using BM MSC. More intriguingly, however, we found that the sustained exposure of OSM kept the expression of Alpl at a high level while it suppressed the induction of Bglap2, a terminal differentiation marker, even after 20 days of induction (Fig. 3C). These results strongly suggested that OSM induces osteogenic differentiation of PαS cells but suppresses their terminal differentiation.

To further confirm the inhibitory effect of OSM on osteogenic terminal differentiation of PαS cells, we reexamined it in the presence of Dexamethasone (Dex), which has been reported to induce both early and late stages of osteogenic differentiation of BM stromal cells [34, 35]. Similar to the experiment without Dex, the expression levels of Alpl and Spp1 were significantly upregulated 7 days after induction in the presence of OSM, whereas that of Bglap2 was markedly suppressed (Fig. 3E). Given that immature osteolineage cells, rather than more differentiated osteoblasts, are responsible for hematopoietic microenvironment to regulate HSPC proliferation and differentiation [36], OSM may contribute to the constitution of the niche by stimulating the generation of osteolineage progenitors from PαS cells.